PHYSICAL REVIEW D VOLUME 47, NUMBER 5 1 MARCH 1993

Threshold effects on heavy quark production in $\gamma\gamma$ interactions

O. J. P. Éboli
Instituto de Física, Universidade de São Paulo, Caixa Postal 20516, CEP 01498 São Paulo, Brazil

M. C. Gonzalez-Garcia and F. Halzen
Physics Department, University of Wisconsin, Madison, Wisconsin 53706

S. F. Novaes
Instituto de Física Teórica, Universidade Estadual Paulista, Rua Pamplona 145, CEP 01405-900 São Paulo, Brazil
(Received 22 May 1992; revised manuscript received 30 October 1992)

The exchange of gluons between heavy quarks produced in e^+e^- interactions results in an enhancement of their production near threshold. We study QCD threshold effects in $\gamma\gamma$ collisions. The results are relevant to heavy quark production by beamstrahlung and laser backscattering in future linear collider experiments. Detailed predictions for top-, bottom-, and charm-quark production are presented.

PACS number(s): 13.65.+i, 14.40.Gx, 29.27.Bd, 41.75.Ht

I. INTRODUCTION

The QCD threshold enhancement of heavy quark production in e^+e^- [1,2] and hadronic collisions [3] has been profusely studied. In this paper we analyze this effect in $\gamma\gamma$ collisions and we find a significant enhancement of top-quark production at future linear colliders. We consider two possibilities for the sources of photons in an e^+e^- machine: beamstrahlung and laser backscattering.

In studying the prospects for the commissioning of future e^+e^- linear colliders [4], it has become clear that their physics exploitation is inevitably affected by the fact that very dense electron and positron bunches are also a very luminous source of photons. The strong electromagnetic fields associated with the high charge density in such bunches subject particles to very strong accelerating forces just prior to or during the collision. As a result photons are radiated. This is known as beamstrahlung [5–7]. The photon luminosity generated by beamstrahlung depends on the characteristics of the beams, in particular on their transverse shape, the length of the bunches, the number of electrons per bunch, and the nominal beam energy. The desired photon luminosity can, in fact, be achieved by tuning these parameters. We will focus our attention on the design for the 500 GeV Next Linear Collider (NLC) [8, 9], which is the set G of parameters of Ref. [9], and occasionally illustrate how results change for different beam profiles and increased energy.

Beamstrahlung photons have a relatively soft spectrum. Hard photons can be obtained by laser backscattering. Here intense γ beams are generated by backward Compton scattering of soft photons from a laser of a few eV energy [10]. The luminosity distribution over the $\gamma\gamma$ invariant mass is broad and contains an abundant number of very energetic photons. The angular spread from the Compton collision is small compared to the intrinsic spread of the original electron beam and, therefore, the hard photon beam has approximately the same cross-sectional area as the original electron beam.

The enhanced two-photon luminosity, whether from beamstrahlung or laser back-scattering origin, is the source of a large number of $q\bar{q}$ pairs via two distinct mechanisms. The quarks can be generated by a direct photon process, where the photons couple directly to charged quarks. Alternatively, photons can interact via their quark and gluon constituents [11]. This is referred to as a "resolved" photon process. The interaction of high energy photons via their quark or gluon structure leads to the abundant production of hadron secondaries, thus giving rise to an underlying event which gives the once clean e^+e^- event the appearance of a hadron collider interaction [12]. Similarly the production of heavy quarks by the two-photon process sprays the interaction region with a blizzard of charm and beauty quarks and their associated prompt leptons [13]. Two-photon processes also provide unique physics opportunities such as the enhanced production of top quarks [13]. We revisit this problem paying particular attention to QCD enhancement of the threshold production of the top quark in the $\gamma\gamma$ process.

The layout of this paper is as follows. In Sec. II we briefly review the main features of heavy quark production by photons. In Sec. III we exhibit explicit expressions for the differential luminosities dL_{ij}/dz for different sources of photons and partons. The implementation of the QCD corrections for heavy quark production near threshold are discussed in Sec. IV. Section V contains our results and finally we summarize our conclusions in Sec. VI.

II. HEAVY QUARK PRODUCTION IN $\gamma\gamma$ COLLISIONS

The production of heavy quarks in $\gamma\gamma$ collisions can proceed either by direct photons or by "resolved" pho-

tons. "Resolved" photons produce heavy quark pairs via their quark and gluon constituents, which are described in terms of the structure function of the partons in the photon [11]. At the tree level, there are four distinct contributions to heavy quark pair production:

$$\begin{aligned} &\gamma+\gamma \to Q\bar{Q}, \\ &\gamma+\gamma(g) \to Q\bar{Q}, \\ &\gamma(g)+\gamma(g) \to Q\bar{Q}, \\ &\gamma(q)+\gamma(\bar{q}) \to Q\bar{Q}, \end{aligned} \tag{1}$$

where $\gamma(g)$ and $\gamma(q)$ denotes a gluon or a quark component of the photon respectively. The expressions for these cross sections are well known and can be found elsewhere [14].

The total cross section is obtained by folding the elementary cross section for the processes (1) with the photon luminosity

$$\sigma(e^+e^- \to \gamma\gamma \to i+j \to Q\bar{Q})(s)$$

$$= \int_{z_{\min}}^{z_{\max}} dz \, \frac{dL_{ij}}{dz} \hat{\sigma}(i+j \to Q\bar{Q}) \quad (\hat{s}=z^2 s). \tag{2}$$

Here $z^2=\tau=\hat{s}/s$, where s is the total e^+e^- c.m. energy squared and $\hat{s}$ the ij pair c.m. energy squared, and dL_{ij}/dz stands for the differential luminosity of the partons i and j.

In order to obtain the total cross section, we must fix the characteristic scales of the coupling constants and structure functions. We evaluate all photon structure functions at the scale $Q^2=\hat{s}/4$. The running strong coupling constant is determined by the renormalization group equation

$$\frac{d\alpha_s(Q^2)}{d\ln Q^2} = -b_0\alpha_s^2 - b_1\alpha_s^3 + O(\alpha_s^3)\,, \tag{3}$$

with

$$b_0 = \frac{33-2N_f}{12\pi}, \qquad b_1 = \frac{153-19N_f}{24\pi^2}\,, \tag{4}$$

where N_f is the number of active flavors. For tree-level cross sections we will use the first-order ($b_1=0$) solution

$$\alpha_s(Q^2) = \frac{12\pi}{(33-2N_f)\ln(Q^2/\Lambda_n^2)}. \tag{5}$$

At second-order we will solve Eq. (3) numerically. Flavor thresholds are incorporated by choosing an appropriate value for Λ_n which guarantees that α_s is continuous through the thresholds $Q^2=m_i^2$ for $i=c,b,t$. Different values of Λ_4 will be chosen corresponding to the different parametrizations of the photon structure functions. Finally, we employ a running electromagnetic coupling, which in our energy range is well described by

$$\alpha_{\rm em} = \frac{1}{128-\frac{40}{9\pi}\ln(\sqrt{\hat{s}}/M_Z)}\,. \tag{6}$$

III. DISTRIBUTION FUNCTIONS

The interpenetration of the dense electron and positron bunches in future e^+e^- colliders generates strong accelerations on the electrons and positrons near the interaction point. This acceleration gives rise to abundant bremsstrahlung. This phenomenon is known as beamstrahlung [5–7], and the distribution function of photons created this way can be written in the form

$$F^B_{\gamma/e}(x,b) = F^{(-)}_{\gamma/e}(x,b)\,\Theta(x_c-x) + F^{(+)}_{\gamma/e}(x,b)\,\Theta(x-x_c)\,. \tag{7}$$

Here x is the fraction of the beam energy carried by the photon, b is the impact parameter of the produced γ, and x_c separates low and high photon-energy regions where different approximations to $F^B_{\gamma/e}$ are used. The distribution $F^{(-)}_{\gamma/e}$ adequate for small and intermediate values of x is given by [6, 8]

$$F^{(-)}_{\gamma/e}(x,b) \simeq \frac{CK}{\Upsilon^{1/3}}\left[\frac{1+(1-x)^2}{x^{2/3}(1-x)^{1/3}}\right]\left\{1+\frac{1}{6C\Upsilon^{2/3}}\left(\frac{x}{1-x}\right)^{2/3}\exp\left[\frac{2}{3\Upsilon}\frac{x}{(1-x)}\right]\right\}^{-1}, \tag{8}$$

where $C=-\mathrm{Ai}'(0)=0.2588$, and $\mathrm{Ai}(x)$ is the Airy's function. On the other hand, for large values of x, we have

$$F^{(+)}_{\gamma/e}(x,b) \simeq \frac{K}{2\sqrt{\pi}\Upsilon^{1/2}}\left[\frac{1-x(1-x)}{x^{1/2}(1-x)^{1/2}}\right] \times \exp\left[-\frac{2}{3\Upsilon}\frac{x}{(1-x)}\right]. \tag{9}$$

The value x_c in Eq. (7) is such that $F^B_{\gamma/e}$ is continuous at $x=x_c$, i.e., $F^{(-)}_{\gamma/e}(x_c,b)=F^{(+)}_{\gamma/e}(x_c,b)$. The value of x_c depends on the machine design, e.g., $x_c\simeq 0.48$ for the original design for NLC. The dimensionless quantities K and Υ are defined as

$$\begin{aligned} K &\equiv 2\sqrt{3}\alpha\frac{\sigma_z E_\perp}{m}\,, \\ \Upsilon &\equiv \frac{pE_\perp}{m^3}\,, \end{aligned} \tag{10}$$

where m and p are the electron mass and momentum, and $E_\perp$ is the transverse electric field inside a uniform elliptical bunch of dimensions $l_{x,y}=2\sigma_{x,y}$ and $l_z=2\sqrt{3}\sigma_z$:

$$E_\perp = \frac{N\alpha}{2\sqrt{3}(\sigma_x+\sigma_y)\sigma_z}\left(\frac{b_x^2}{\sigma_x^2}+\frac{b_y^2}{\sigma_y^2}\right)^{1/2}, \quad (11)$$

where N is the number of particles in the bunch. For the original NLC design the value of these parameters is $\sigma_x = 1.7\times10^{-5}$ cm, $\sigma_y = 6.5\times10^{-7}$ cm, $\sigma_z = 0.011$ cm, and $N = 1.67\times10^{10}$. We also study the effect of tuning to round beams by choosing $\sigma_{x(y)} = 3.3\times10^{-6}$ cm. For this case $x_c \simeq 0.64$.

Notice that $F^B_{\gamma/e}(x,b)$ depends on the impact parameter through K and Υ. In $\gamma\gamma$ collisions we should average over the impact parameters in order to obtain the actual photon-photon luminosity:

$$\frac{dL^B_{\gamma\gamma}}{dz} = 2z\int\frac{d^2b}{4\pi\sigma_x\sigma_y}\int_{z^2}^1\frac{dx}{x}F^B_{\gamma/e}(x,b)F^B_{\gamma/e}(z^2/x,b)\,. \quad (12)$$

Therefore the necessity to average over the impact parameter implies that we cannot decompose the effect of beamstrahlung into photon structure functions [8].

The photon luminosity of beamstrahlung is very sensitive to the transverse shape of the beam [6]. The aspect ratio

$$G = \frac{\sigma_x+\sigma_y}{2\sqrt{\sigma_x\sigma_y}}$$

provides a good measure of beamstrahlung, with large photon luminosities associated with small values of G. For high photon luminosity one tunes to round beams, i.e., $G = 1$. For the NLC original design $G \simeq 2.7$ [8, 9].

Conventional bremsstrahlung of photons by electrons further contributes to the photon luminosity. This can be computed in the lowest-order approximation using the well-known Weiszäcker-Williams distribution

$$F_{\rm WW}(x,E_{\rm max}) = \frac{\alpha}{2\pi}\frac{1+(1-x)^2}{x}\ln\left(\frac{E^2_{\rm max}}{m_e^2}\right), \quad (13)$$

where $E_{\rm max}$ is the electron beam energy. The total γ distribution is obtained by adding $F_{\rm WW}$ to the beamstrahlung distribution function $F^B_{\gamma/e}$.

The logarithm in Eq. (13) arises from the integration over the momentum squared (p^2) of the photon propagator up to the maximum value $E^2_{\rm max} = s/2$. When computing cross sections we fold this distribution with an elementary cross section which is evaluated for on-shell photons. The effective photon approximation is valid only in the kinematical regime where the elementary cross section does not depend on p^2. It overestimates the number of off-shell photons. In order to avoid this, we introduce a cutoff $E_{\rm max} = E_{\rm cut}$ in the integration over the photon propagator which guarantees that the effective photon approximation is used only in the kinematic range where it is strictly valid. $E_{\rm max}$ will be in general process dependent: in direct $\gamma\gamma$ we will use the transverse momentum of the heavy quark as a cutoff, otherwise we choose $E_{\rm max} = 1$ GeV. This procedure makes the evaluation of the luminosities and cross sections conservative.

Abundant large invariant mass photons can also be obtained by the process of laser backscattering. When a laser light is focused almost head to head on an energetic electron or positron beam we obtain a large quantity of photons carrying a great amount of the fermion energy. The energy spectrum of backscattered laser photons is [15]

$$F^L_{\gamma/e}(x,\xi) \equiv \frac{1}{\sigma_c}\frac{d\sigma_c}{dx} = \frac{1}{D(\xi)}\left[1-x+\frac{1}{1-x}-\frac{4x}{\xi(1-x)}+\frac{4x^2}{\xi^2(1-x)^2}\right], \quad (14)$$

where σ_c is the total Compton cross section. For the photons going in the direction of the initial electron, the fraction x represents the ratio between the scattered photon and the initial electron energy ($x = \omega/E$). In Eq. (14), we defined

$$D(\xi) = \left(1-\frac{4}{\xi}-\frac{8}{\xi^2}\right)\ln(1+\xi)+\frac{1}{2}+\frac{8}{\xi}-\frac{1}{2(1+\xi)^2}, \quad (15)$$

with

$$\xi \equiv \frac{4E\omega_0}{m^2}\cos^2\frac{\alpha_0}{2} \simeq \frac{2\sqrt{s}\omega_0}{m^2}, \quad (16)$$

where ω_0 is the laser photon energy and ($\alpha_0 \sim 0$) is the electron-laser collision angle. The maximum value of x is

$$x_m = \frac{\omega_m}{E} = \frac{\xi}{1+\xi}\,. \quad (17)$$

From Eq. (14) we can see that the fraction of photons with energy close to the maximum value grows with E and ω_0. Usually, the choice of ω_0 is such that it is not possible for the backscattered photon to interact with the laser and create e^+e^- pairs, otherwise the conversion of electrons to photons would be dramatically reduced. In our numerical calculations, we assumed $\omega_0 \simeq 1.26$ eV for the NLC which is below the threshold of e^+e^- pair creation ($\omega_m\omega_0 < m^2$). Thus for the NLC beams we have $\xi \simeq 4.8$, $D(\xi) \simeq 1.9$, and $x_m \simeq 0.83$. In this case, half or more of the scattered photons are emitted inside a small angle ($\theta < 5\times10^{-6}$ rad) and are very energetic ($\omega > 100$ GeV).

The $\gamma\gamma$ luminosity from laser backscattering is then

$$\frac{dL^L_{\gamma\gamma}}{dz} = 2zk^2\int_{z^2/x_m}^{x_m}\frac{dx}{x}F^L_{\gamma/e}(x,\xi)F^L_{\gamma/e}(z^2/x,\xi)\,, \quad (18)$$

where the conversion coefficient k represents the average number of high-energy photons per one electron. We assume $k = 1$ in our calculations.

Figure 1(a) contains the differential $\gamma\gamma$ luminosities. Beamstrahlung luminosity is shown for two different aspect ratios (G) of the beam at the NLC energies. In order to show the bremsstrahlung contribution, we plotted

the $\gamma\gamma$ luminosity for beamstrahlung with and without considering the bremsstrahlung photons. The actual $\gamma\gamma$ luminosity will be somewhat reduced because no $E_{\max}$ cutoff was implemented in the bremsstrahlung contribution in this figure. It is interesting to notice the very steep dependence of the luminosity on z. In this figure we have also shown the differential luminosity, Eq. (18), for laser backscattering. This luminosity is roughly constant in most of the $z < x_m$ range, as a consequence of the hard photon spectrum.

The luminosities shown in Fig. 1(a) are valid for interactions where the photon couples directly to the quarks. Interactions initiated by "resolved" photons are described in terms of structure function of partons, quarks, and gluons, inside the photon [11]. We define an effective distribution of partons in the electron by folding the photon structure functions with the photon distribution in the electrons:

$$F_{p/e}^{L,B}(x,Q^2) = \int_x^1 \frac{dy}{y} F_{\gamma/e}^{L,B}(x) P^{\gamma}(x/y,Q^2) \,, \qquad (19)$$

where $P^{\gamma} = q^{\gamma}$ (G^{γ}) is the quark (gluon) structure function. Here, we also add the bremsstrahlung photons to the beamstrahlung ones, and in this case an additional integration over impact parameter must be performed. For "resolved" photons the natural cutoff on the bremsstrahlung contribution is of order $\Lambda_{\rm QCD}$. We use $E_{\rm cut} = 1$ GeV. Also, the suppression of the parton content of highly off-shell photons is not a problem with this choice, since we evaluate the parton distributions at $Q^2 = \hat{s}/4$ with $Q^2 > E_{\rm cut}^2$, which guarantees that we do not include highly off-shell photons.

Finally, we define the parton-parton luminosity for once and twice "resolved" photons as

$$\frac{dL_{ij}^{L,B}}{dz} = 2Nz \int_{z^2/x}^1 \frac{dx}{x} F_{i/e}^{L,B}(x) F_{j/e}^{L,B}(z^2/x) \,, \qquad (20)$$

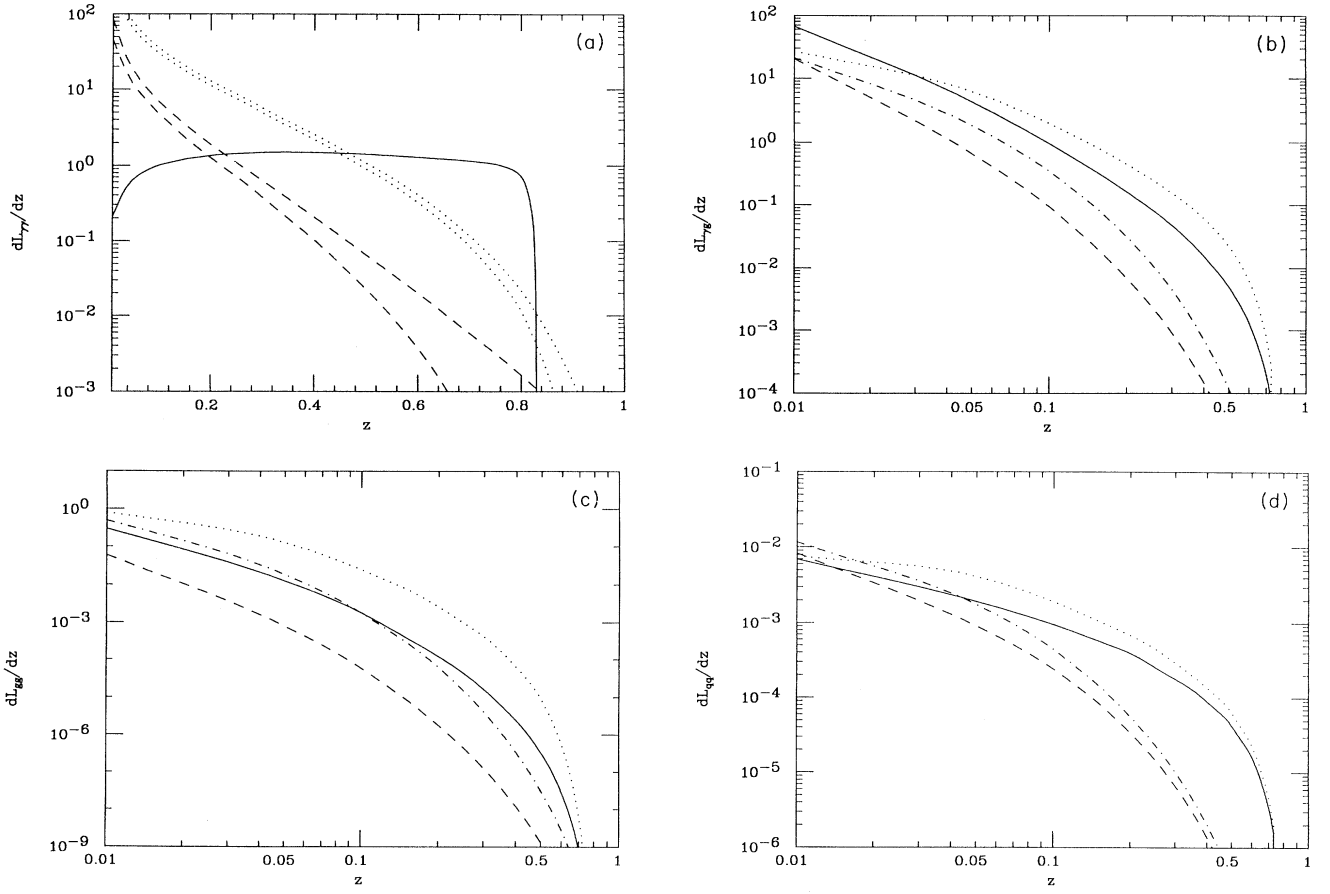

FIG. 1. Differential luminosities in $\gamma\gamma$ collisions at $\sqrt{s} = 500$ GeV. In (a) the direct photon luminosities are shown for backscattered laser photons (solid line), beamstrahlung photons for "ribbonlike" beam with G=2.7 (dashed lines), and round beam (dotted lines). The lower dashed and dotted lines show the luminosity without including the bremsstrahlung photons and the upper ones include the bremsstrahlung photons according to the EPA distribution of Eq. (13). In (b) the once "resolved" γg luminosities are shown for backscattered laser photons (solid and dotted lines) and beamstrahlung for "ribbonlike" beam (dashed and dot-dashed lines). The solid and dashed lines correspond to the DG parametrization of partons inside the photons and the dotted and dot-dashed ones correspond to the LAC3 parametrization. (c) and (d) show the twice "resolved" gg and $q\bar{q}$ luminosities for the same cases as (b).

where $i = \gamma$, $j = g$ for once "resolved" luminosity, and $i = j = g$ or $i = q$ and $j = \bar{q}$ for twice "resolved" luminosities. The statistical factor N assumes the value $N = 2$ for distinct partons ($i \neq j$) and $N = 1$ for identical partons ($i = j$).

The structure functions for partons inside the photon, $q^\gamma(x, Q^2)$ and $G^\gamma(x, Q^2)$, are obtained for a given value of $Q^2 = Q_0^2$ by fitting the experimental data [16]. The Q^2 evolution is obtained, as usual, by solving an inhomogeneous set of Altarelli-Parisi equations [17, 18]. Several parametrizations have been proposed in the literature [17, 19, 20]. They lead to different predictions as a consequence of the large uncertainties due to the small number of experimental results. In particular very different parametrizations for $G^\gamma(x, Q^2)$ can fit the data. We will present predictions for the parametrizations of Drees-Grassie (DG) [19] and Levy-Abramowicz-Charchula (LAC3) [17], which are respectively characterized by a soft and a hard gluon distribution. We take $\Lambda_4 = 0.4$ GeV for the DG parametrization of the photon structure functions and $\Lambda_4 = 0.2$ GeV for the LAC parametrizations.

In Fig. 1(b) we show the once "resolved" γg luminosities for backscattered laser photons and beamstrahlung for "ribbonlike" beams, using DG and LAC3 parametrizations of the parton distributions. This figure illustrates well the different behavior of the distributions DG and LAC3: for backscattered photons, the LAC3 γg luminosity is larger (smaller) than the corresponding one for DG at large (small) z.

Figures 1(c) and 1(d) show the twice "resolved" gg and $q\bar{q}$ luminosities (summed over the light quark flavors). LAC3 parametrization predicts a twice "resolved" luminosity always larger than the one obtained with the DG parametrization.

IV. THRESHOLD BEHAVIOR

The exchange of gluons between associatively produced heavy quarks modifies significantly their production cross section near the threshold. Moreover, for a very heavy quark, such as the top quark, nonperturbative QCD effects are small, and the threshold behavior can be computed perturbatively [21, 22], since the top-quark width acts as an infrared cutoff . In this case, the modification of the cross section near threshold due to QCD can be calculated in terms of a Coulomb-like interaction between t and $\bar{t}$.

In $\gamma\gamma$ collisions the $t\bar{t}$ pair can be produced in either a color singlet or an octet state, depending on the production mechanism. The threshold interaction between the t and $\bar{t}$ can be described by an attractive Coulomb-like potential

$$V_S(r) = -\frac{4}{3}\frac{\alpha_s}{r} \tag{21}$$

in the color singlet channel, and by a repulsive potential

$$V_8(r) = \frac{1}{6}\frac{\alpha_s}{r} \tag{22}$$

in the color octet state. Since the interaction is attractive in the singlet channel, the formation of bound states by multiple gluon exchanges between the t and the $\bar{t}$ can in principle occur. However, if the top quark is heavier than ~ 140 GeV, the formation time of the bound state by gluon exchange is larger than the lifetime of toponium and the resonance structure disappears [21, 23]. These interactions nevertheless lead to a significant modification of the cross section near threshold. This mechanism is analogous to the Coulomb rescattering in QED discussed by Sommerfeld [24] and Sakharov [25].

In the narrow width approximation, we can obtain the QCD effects near the threshold replacing, in the tree-level cross sections, the usual threshold factor

$$\beta = \sqrt{1 - \frac{4m_t^2}{\hat{s}}}\,, \tag{23}$$

by

$$\beta|\Psi_{S,8}(0)|^2 = \beta\frac{X_{S,8}}{1 - \exp(-X_{S,8})} \equiv \beta R_{S,8}\,, \tag{24}$$

where $\Psi_{S,8}(0)$ is the wave function at the origin and

$$X_S = \frac{4}{3}\frac{\pi\alpha_s}{\beta}\,, \qquad X_8 = -\frac{1}{6}\frac{\pi\alpha_s}{\beta}\,, \tag{25}$$

for the color singlet state (S), and octet (8) channels respectively.

Equation (24) can be interpreted as the exponentiated version of the first-order QCD corrections near the threshold. The first term in its expansion in powers of α_s coincides with the one-loop QCD corrections. The expression (24) does not include the effects of bound states below threshold [2, 3]. These states are confined into a very small energy region and their contribution to the total cross section, which is obtained by integration over all c.m. energies, is rather small. Furthermore, unlike the e^+e^- machines, it is not possible to observe the effect of bounds states in the cross section through the $t\bar{t}$ excitation curve due to the smearing introduced by the parton distribution functions.

Near threshold ($\beta \to 0$), the cross section in the color singlet channel is increased since β is substituted by the nonvanishing factor $4\pi\alpha_s/3$. On the other hand, the octet channel cross section is exponentialy suppressed in this limit. Therefore, the factors in Eq. (24) are large, especially in the color singlet channel, and this gives rise to a substantial enhancement of the production cross section.

When computing the $t\bar{t}$ cross sections we use α_s in Eq. (5). The tree-level cross sections are evaluated at $Q^2 = \hat{s}/4$ while the QCD enhancement is given at

$$Q^2 = p_{\rm top}^2 = m_t\sqrt{E^2 + \Gamma_t^2} + \frac{E^4}{4}\,, \tag{26}$$

where $E = \sqrt{\hat{s}} - 2m_t$. We thus include the effect of the finite top width $\Gamma_t \approx 175\, m_t^3/M_W^3$ MeV.

In $\gamma\gamma$ collisions we have four contributions to top production [see Eq. (1)]. In the direct $\gamma\gamma$ interactions, the $t\bar{t}$ pair is produced in a singlet state. Therefore the elementary cross section must be replaced by

$$\sigma^{\rm th}(\gamma\gamma \to t\bar{t}) = \sigma_0(\gamma\gamma \to t\bar{t})R_S \ , \tag{27}$$

where σ_0 is the Born cross section. In $\gamma(g)+\gamma$ collision the $t\bar{t}$ is produced in the color octet channel because the gluon is a color octet. The same is true in $\gamma(q)+\gamma(\bar{q})$ annihilation where a gluon is exchanged in the s channel. In these cases we have

$$\sigma^{\rm th}(q\bar{q}\ (\gamma g) \to t\bar{t}) = \sigma_0(q\bar{q}\ (\gamma g) \to t\bar{t})R_8 \ . \tag{28}$$

In $\gamma(g)+\gamma(g)$ fusion the final state is a mixture of color singlet and octet states in a ratio 2 to 5 given by the color factors. Therefore, we are led to

$$\sigma^{\rm th}(gg \to t\bar{t}) = \sigma_0(gg \to t\bar{t})\left(\frac{2}{7}R_S + \frac{5}{7}R_8\right) \ . \tag{29}$$

Since the enhancement in the singlet channel is much larger than the suppression in the octet channel the net correction to gg is positive. For the sake of comparison we also include the cross sections for top production in direct e^+e^- annihilation. $t\bar{t}$ pairs produced in this channel are in the color singlet state. Therefore we will have

$$\sigma^{\rm th}(e^+e^- \to t\bar{t}) = R_S\sigma_0(e^+e^- \to t\bar{t}). \tag{30}$$

The previous analysis, valid for nonrelativistic particles, cannot be applied to charm and bottom production. In this case bound state effects play a critical role and the computation of the QCD enhancement becomes nonperturbative near threshold. Here, we will compute the full $O(\alpha^2\alpha_s)+O(\alpha\alpha_s^2)+O(\alpha_s^3)$ inclusive cross section, $\gamma\gamma \to Q\bar{Q}[g,q,\bar{q}]$ [27, 26], in the modified minimal subtraction ($\overline{MS}$) scheme as defined in [26]. We use the value of α_s obtained by solving Eq. (3) at second order. We will show the results for two different scales $Q^2 = m_i^2$ and $Q^2 = 4m_i^2$, $i = c, b$. This procedure does not incorporate bound-state effects but should nevertheless represent an adequate estimate of the effect of the threshold enhancement. The results will indicate that these corrections are small relative to the uncertainty associated with the charm- and bottom-quark masses. Again, we include the tree level and one-loop cross sections for charm and bottom production in direct e^+e^- annihilation. The one-loop cross section is given by [28]

$$\sigma^{1\ \rm loop}_{e^+e^-} = \left[1+\frac{4}{3}\alpha_s f(\beta)\right]\sigma^0_{e^+e^-} \ . \tag{31}$$

The function $f(\beta)$ [29] is rather complicated involving several Spence functions. Schwinger [29] has constructed the interpolating formula

$$f(x) = \frac{\pi}{2x} - \frac{3+x}{4}\left(\frac{\pi}{2} - \frac{3}{4\pi}\right) \tag{32}$$

which agrees with the exact result to 1% in the interval of interest.

V. RESULTS

We are now ready to perform a full computation of heavy quark production in $\gamma\gamma$ interaction including direct and "resolved" photons and incorporating QCD corrections near threshold. In Table I we list the production cross sections for top assuming $m_{\rm top} = 120$ GeV and $\sqrt{s} = 500$ GeV. Contributions from different subprocesses are shown separately, with and without threshold factors included for the sake of comparison. Results are shown for beamstrahlung, laser backscattering, and direct e^+e^- production.

As pointed out in Ref. [12], in the case of top production the contribution of "resolved" photons to the total $\gamma\gamma$ cross section is small as a result of the suppression of their luminosity at high values of x, as can be seen from Fig. 1. Even for the LAC3 parametrization, characterized by a very hard gluon spectrum, the contribution is at most 3% for $\sqrt{s} = 500$ GeV. Since the direct singlet channel dominates, the threshold effect results in a significant enhancement of the total cross section. This

TABLE I. Cross sections for $t\bar{t}$ production at $\sqrt{s} = 500$ GeV for $m_t = 120$ GeV. The first row corresponds to e^+e^- annihilation production and the others correspond to photon-photon production. For each process the left (right) column is the cross section without (with) the threshold factors. We separate the different contributions to the photon-photon cross sections from direct photons, $\gamma+\gamma$, once "resolved" gluon-photon fusion, $\gamma+\gamma(g)$, and twice "resolved" gluon fusion, $\gamma(g)+\gamma(g)$, and $\gamma(q)+\gamma(\bar{q})$ annihilation. For "resolved" photon processes the upper number is the cross section with DG parametrization and the lower one is the cross section with LAC3 parametrization.

Process	Cross section (pb)					
e^+e^-	0.70			0.94		
Photon-photon	Laser		G=2.7		G=1	
$\gamma+\gamma$	0.74	1.2	9.0×10^{-3}	1.8×10^{-2}	0.18	0.36
$\gamma+\gamma(g)$	4.2×10^{-3}	3.8×10^{-3}	1.2×10^{-5}	1.1×10^{-5}	3.5×10^{-4}	3.1×10^{-4}
	1.7×10^{-2}	1.5×10^{-2}	4.8×10^{-5}	4.4×10^{-5}	1.4×10^{-3}	1.3×10^{-3}
$\gamma(g)+\gamma(g)$	5.4×10^{-7}	7.1×10^{-7}	1.4×10^{-9}	1.8×10^{-9}	3.1×10^{-8}	4.2×10^{-8}
	9.7×10^{-6}	1.2×10^{-5}	2.4×10^{-8}	3.1×10^{-8}	5.5×10^{-7}	7.2×10^{-7}
$\gamma(q)+\gamma(\bar{q})$	2.5×10^{-4}	2.2×10^{-4}	8.8×10^{-7}	7.8×10^{-7}	2.6×10^{-5}	2.3×10^{-5}
	2.8×10^{-4}	2.5×10^{-4}	9.7×10^{-7}	8.7×10^{-7}	2.9×10^{-5}	2.6×10^{-5}

enhancement is roughly a factor of 2 for beamstrahlung and more than 50% for laser backscattering.

In Fig. 2 we show the invariant mass distribution of the $t\bar{t}$ pair. The modifications due to threshold effects are larger for small invariant masses, corresponding to $t\bar{t}$ pair production near threshold. This explains why the QCD corrections are larger in $\gamma\gamma$ than in e^+e^- production. For the same reason the correction is small for laser backscattering where the luminosity at low x is suppressed. Despite the fact that the corrections look big far from threshold we have checked that at least 93% of the effect in the total cross section comes from the region of invariant mass less than $m_{\rm top}$ above threshold.

The dependence on the top mass and on the collider energy is shown in Fig. 3. As expected, the QCD corrections increase slightly with the mass and decrease with the c.m. energy. As pointed out in Ref. [13] beam-

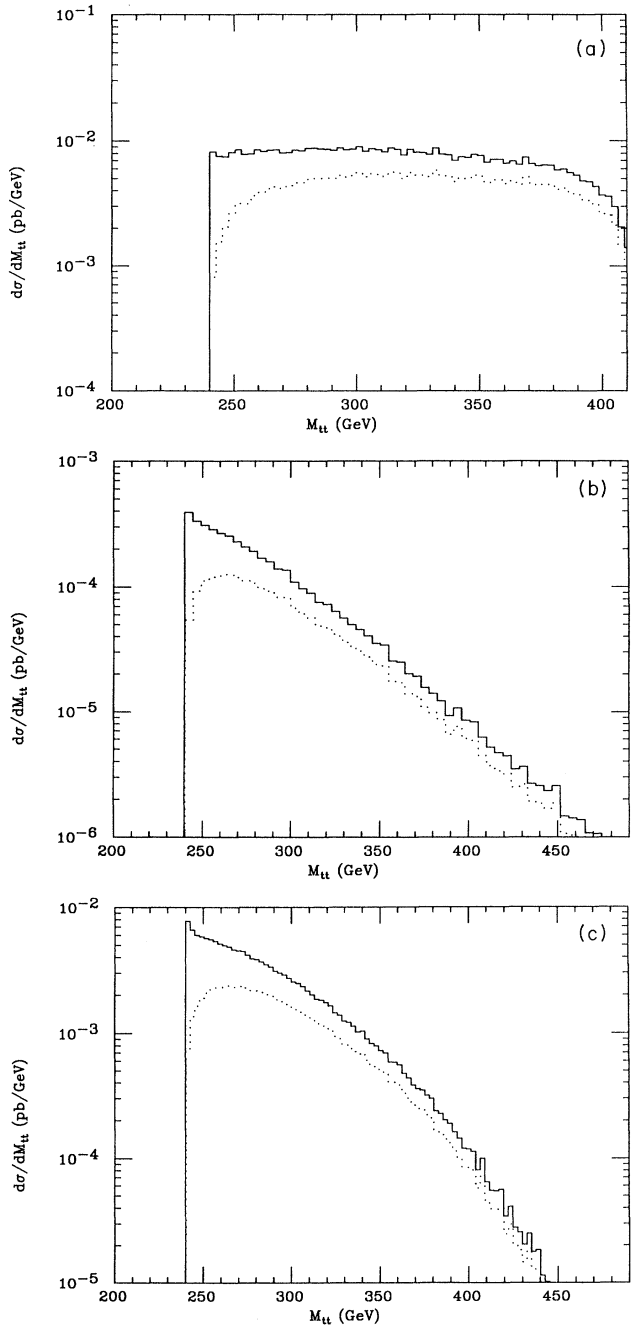

FIG. 2. Invariant mass distributions of the $t\bar{t}$ pairs produced in $\gamma\gamma$ collisions for $m_t = 120$ GeV. (a) corresponds to backscattered laser photons while (b) and (c) correspond to beamstrahlung photons for G=2.7 and G=1, respectively. In all cases the solid (dotted) lines show the distributions with (without) the threshold factors.

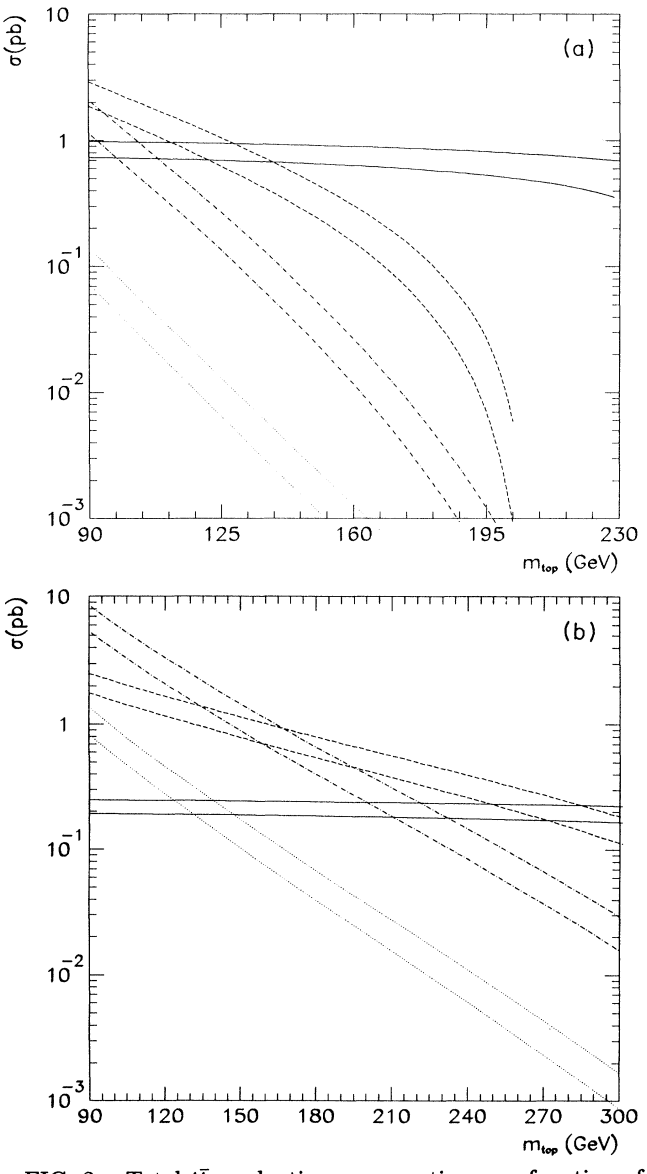

FIG. 3. Total $t\bar{t}$ production cross section as a function of m_t for $\sqrt{s} = 500$ GeV (a) and $\sqrt{s} = 1$ TeV (b). Solid lines are the cross sections for direct e^+e^- production, dashed lines for $\gamma\gamma$ production with backscattered laser photons, and dotted (dot-dashed) lines for $\gamma\gamma$ production with beamstrahlung photons with G=2.7 (G=1). In all cases the upper (lower) lines show the cross section with (without) the threshold factors.

strahlung, for round beams, can give a substantial contribution to $t\bar{t}$ production. The threshold corrections make this contribution even larger. At $\sqrt{s} = 500$ GeV the two photon contributions are at most 10% for the "ribbonlike" design. However, for a circular beam more than 50% of the $t\bar{t}$ pairs with $m_{\rm top} < 110$ GeV are produced in two photon collisions. Since the $\gamma\gamma$ cross section increases with energy while the e^+e^- one decreases, the two photon contributions are much more important at 1 TeV. However top quarks produced by beamstrahlung photons preferentially populate the low p_T region and so do the prompt leptons from their decay [see Figs. 4(a) and 4(b)]. In this case their signature suffers from a large background from b and c produced both in direct e^+e^- annihilation and in two photon processes.

The advantage of photon interactions is more dramatic for laser backscattering. We first notice that at $\sqrt{s} = 500$ (1000) GeV, for $m_{\rm top} < 130$ (250) GeV, a "$\gamma\gamma$ collider"

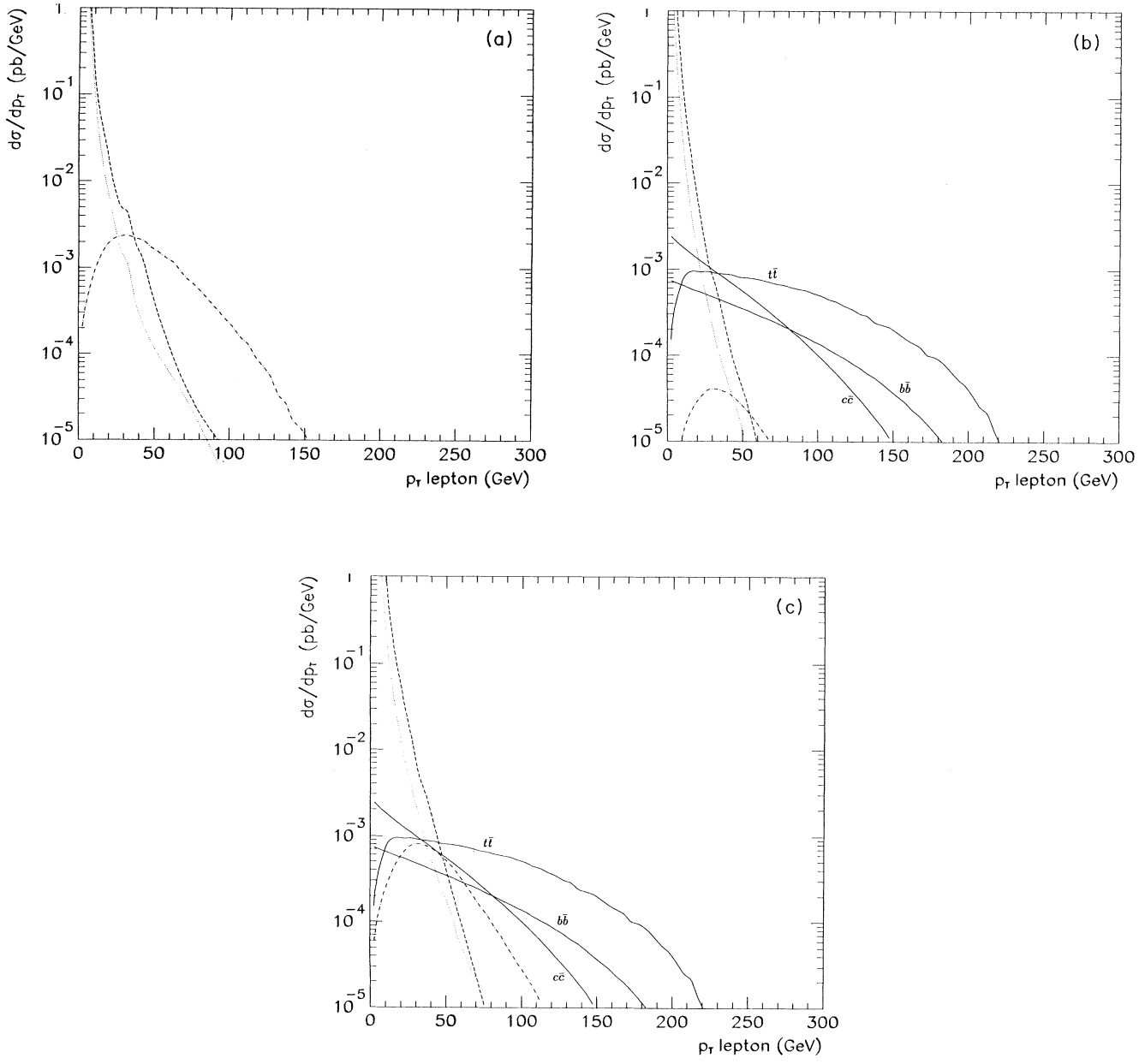

FIG. 4. Transverse momentum distribution of the lepton produced in the heavy quark decay. Dashed, dotted, and dot-dashed lines correspond respectively to charm, bottom, and top produced in $\gamma\gamma$ process with backscattered laser photons (a) and beamstrahlung photons for G=2.7 (b) and G=1 (c). Solid lines correspond to annihilation production of the heavy quarks according to labels in the figure. Quark masses were assumed to be $m_c = 1.86$ GeV, $m_b = 5.2$ GeV, and $m_t = 120$ GeV.

can produce more $t\bar{t}$ pairs than the corresponding e^+e^- collider . The background from c and b quarks can be efficiently suppressed because it is concentrated at lower p_T values than the one from the top signal. Furthermore, the separation of the signal from the background is easier in this case than for direct e^+e^- production [compare Figs. 4(a) and 4(b)].

The cross sections at $\sqrt{s} = 500$ GeV for inclusive charm and bottom production are listed in Tables II and III. At order α^3, with $\alpha = \alpha_{\rm em}$ or α_s, there are four new contributions to the inclusive cross section apart from those of Eq. (1): $\gamma\gamma(q[\bar{q}]) \to Q\bar{Q}q[\bar{q}]$ and $\gamma(g)\gamma(q[\bar{q}]) \to Q\bar{Q}q[\bar{q}]$. Note that negative corrections only appear because we have separated the leading-order parton diagram from the QCD corrections; they should be added [26]. The cross sections depend upon various factors, like the quark mass, factorization scale, Λ, and the choice of parametrization of the photon structure functions. Although the corrections to individual channels can be large, the net modification of the total yield of heavy quarks is smaller as a result of cancellation between opposite behaviors of the different channels. Even the sign of the correction depends on the quark mass, the scale of the coupling constant, the photon spectrum, and the parametrization of the photon structure functions.

We show results for two extreme values of the masses $m_c = 1.35$ and 1.86 GeV, and $m_b = 4.5$ and 5.2 GeV. The strong dependence on the mass makes predictions relatively imprecise. In particular, the results are extremely sensitive to the charm mass (by a factor of $\simeq 2$), while for bottom the uncertainty is of the order of 40%. This sensitivity to the heavy quark mass was observed before in hadronic collisions and in ep collisions [26].

The dominant contribution to the total cross section comes from the once "resolved" γg process, due to the large γg luminosity. In order to analyze the dependence on the parametrization of the structure functions we evaluated the cross sections for DG and LAC3 parametrizations. In contrast with the top case, the DG cross sections can be larger than those computed with LAC3 structure functions. This is a result of a smaller Λ_4 value and a harder gluon spectrum in the LAC3 parametrization. In fact, we have checked that LAC1 indeed gives a 5–10 times bigger result for the once "resolved" process since parametrizations with softer spectra give rise to larger cross sections. Moreover, uncertainty in the cross section due to the structure functions is smaller for bottom production than for charm.

Finally, in order to estimate the size of higher-order QCD corrections, we computed cross sections for two different factorization scales: $Q^2 = m_i^2$ and $Q^2 = 4m_i^2$, with $i = c, b$ respectively. For charm production the results vary as much as 50%, while for bottom the variations are of the order of 20%.

Despite the large values of the cross sections for charm and bottom, most of them are produced at very low transverse momentum as shown in Fig. (4). Therefore they will be hard to observe. If we impose a transverse

TABLE II. Same as Table I for charm production. The cross sections are listed for two quark masses. For each process the two right (left) numbers are the tree-level (one loop) cross sections. In each case the left number is for $Q^2 = m_c^2$ and the right one for $Q^2 = 4m_c^2$.

Process	m_c (GeV)	Cross section (nb)					
e^+e^-	1.35 – 1.86	0.77×10^{-3}			$0.83 \times 10^{-3} - 0.87 \times 10^{-3}$		
Photon-photon		Laser		G=2.7		G=1	
$\gamma\gamma$	1.35	0.165	0.365 – 0.305	12.1	19.4 – 17.3	47.0	75.1 – 66.9
	1.86	0.138	0.264 – 0.231	6.68	10.1 – 9.22	26.8	40.1 – 36.8
$\gamma\gamma(g)$	1.35	266 – 170	374 – 151	87.7 – 55.9	104 – 56.0	629 – 401	771 – 390
		96.9 – 71.1	201 – 69.8	66.1 – 49.7	92.2 – 47.0	408 – 299	600 – 282
	1.86	120 – 82.7	151 – 86.8	33.3 – 23.0	38.0 – 25.5	249 – 172	290 – 188
		50.4 – 38.5	82.4 – 37.6	31.2 – 23.8	37.5 – 23.6	194 – 148	246 – 145
$\gamma\gamma(q)$ + $\gamma\gamma(\bar{q})$	1.35	0.0 – 0.0	26.4 – 0.513	0.0 – 0.0	9.18 – (−1.13)	0.0 – 0.0	70.7 – (−5.21)
		0.0 – 0.0	16.6 – 1.24	0.0 – 0.0	6.34 – (−0.674)	0.0 – 0.0	48.2 – (−2.26)
	1.86	0.0 – 0.0	8.11 – (−0.095)	0.0 – 0.0	2.47 – (−0.524)	0.0 – 0.0	19.8 – (−2.80)
		0.0 – 0.0	5.98 – 0.300	0.0 – 0.0	1.95 – (−0.383)	0.0 – 0.0	15.6 – (−1.75)
$\gamma(g)\gamma(g)$	1.35	38.2 – 15.5	51.2 – 18.1	5.44 – 2.21	6.47 – 2.84	49.7 – 20.2	60.4 – 25.1
		48.7 – 26.2	95.7 – 31.7	18.2 – 9.77	24.3 – 11.0	127 – 68.5	185 – 77.1
	1.86	11.2 – 5.34	14.2 – 6.86	1.31 – 0.623	1.55 – 0.855	12.7 – 6.05	15.2 – 8.12
		20.5 – 11.9	31.5 – 13.9	6.54 – 3.81	7.80 – 4.47	47.8 – 27.8	60.0 – 32.3
$\gamma(q)\gamma(\bar{q})$	1.35	0.681 – 0.276	0.225 – 0.173	0.685 – 0.278	0.321 – 0.235	3.89 – 1.58	1.72 – 1.27
		0.304 – 0.164	0.148 – 0.117	0.330 – 0.178	0.165 – 0.139	1.89 – 1.02	0.932 – 0.779
	1.86	0.322 – 0.153	0.143 – 0.116	0.205 – 0.097	0.108 – 0.085	1.28 – 0.607	0.650 – 0.515
		0.159 – 0.092	0.083 – 0.070	0.144 – 0.084	0.078 – 0.069	0.853 – 0.497	0.459 – 0.400
$\gamma(g)\gamma(q)$ + $\gamma(g)\gamma(\bar{q})$	1.35	0.0 – 0.0	15.2 – 0.344	0.0 – 0.0	1.75 – (−0.145)	0.0 – 0.0	17.2 – (−0.762)
		0.0 – 0.0	14.6 – 1.66	0.0 – 0.0	2.81 – 0.043	0.0 – 0.0	23.7 – 1.14
	1.86	0.0 – 0.0	3.15 – (−0.059)	0.0 – 0.0	0.312 – (−0.056)	0.0 – 0.0	3.22 – (−0.039)
		0.0 – 0.0	4.03 – 0.352	0.0 – 0.0	0.659 – (−0.041)	0.0 – 0.0	5.86 – (−0.062)
Total	1.35	305 – 186	467 – 170	106 – 70.5	141 – 75.1	730 – 470	496 – 477
		146 – 97.6	328 – 105	96.7 – 71.7	145 – 74.8	584 – 416	750 – 426
	1.86	132 – 88.3	177 – 93.9	41.5 – 30.4	52.5 – 35.1	290 – 206	369 – 231
		71.2 – 50.6	124 – 52.5	44.6 – 34.4	58.1 – 36.9	269 – 203	368 – 213

TABLE III. Same as Table II for the bottom quark.

Process	m_b (GeV)	Cross section (pb)					
e^+e^-	4.5 – 5.2	0.41			0.44		
Photon-photon		Laser		G=2.7		G=1	
$\gamma\gamma$	4.5	4.91	7.21 – 6.80	74.6	101 – 96.3	332	445 – 425
	5.2	4.43	6.31 – 5.99	55.3	73.9 – 70.9	251	332 – 319
$\gamma\gamma(g)$	4.5	1820 – 1440	2030 – 1600	371 – 293	398 – 343	3030 – 2390	3260 – 2750
		1590 – 1320	1860 – 1340	644 – 533	675 – 574	4430 – 3670	4720 – 3890
	5.2	1140 – 910	1250 – 1010	218 – 175	233 – 205	1810 – 1450	1940 – 1680
		1090 – 915	1240 – 933	409 – 342	426 – 372	2870 – 2400	3020 – 2570
$\gamma\gamma(q)$ + $\gamma\gamma(\bar{q})$	4.5	0.0 – 0.0	99.6 – (−10.2)	0.0 – 0.0	18.7 – (−11.1)	0.0 – 0.0	178 – (−69.8)
		0.0 – 0.0	93.7 – (−5.23)	0.0 – 0.0	17.5 – (−10.9)	0.0 – 0.0	168 – (−66.8)
	5.2	0.0 – 0.0	61.1 – (−7.63)	0.0 – 0.0	10.2 – (−7.27)	0.0 – 0.0	101 – (−47.0)
		0.0 – 0.0	58.9 – (−4.96)	0.0 – 0.0	9.62 – (−7.35)	0.0 – 0.0	96.7 – (−46.8)
$\gamma(g)\gamma(g)$	4.5	287 – 179	331 – 241	21.7 – 13.5	25.1 – 19.6	242 – 151	278 – 213
		1310 – 898	1510 – 1080	244 – 167	269 – 219	2080 – 1430	2300 – 1820
	5.2	156 – 99.8	178 – 135	10.8 – 6.94	12.5 – 10.1	124 – 79.6	143 – 114
		794 – 555	898 – 677	134 – 93.9	148 – 125	1180 – 826	1300 – 1070
$\gamma(q)\gamma(\bar{q})$	4.5	24.1 – 15.0	14.5 – 13.0	10.7 – 6.68	6.63 – 6.02	73.8 – 46.0	45.1 – 40.9
		22.5 – 15.4	14.0 – 12.9	11.9 – 8.19	7.76 – 7.33	80.6 – 55.3	51.7 – 48.6
	5.2	15.7 – 10.1	9.64 – 8.79	6.66 – 4.27	4.20 – 3.88	46.6 – 29.9	29.0 – 26.8
		15.8 – 11.1	10.0 – 9.39	7.70 – 5.39	5.11 – 4.88	53.2 – 37.2	34.8 – 33.1
$\gamma(g)\gamma(q)$ + $\gamma(g)\gamma(\bar{q})$	4.5	0.0 – 0.0	48.9 – (−11.8)	0.0 – 0.0	2.54 – (−2.25)	0.0 – 0.0	33.2 – (−19.9)
		0.0 – 0.0	107 – (−9.68)	0.0 – 0.0	9.06 – (−5.52)	0.0 – 0.0	101 – (−39.6)
	5.2	0.0 – 0.0	24.5 – (−7.52)	0.0 – 0.0	1.09 – (−1.26)	0.0 – 0.0	15.2 – (−11.5)
		0.0 – 0.0	57.3 – (−8.14)	0.0 – 0.0	4.18 – (−3.38)	0.0 – 0.0	49.2 – (−25.5)
Total	4.5	2140 – 1640	2530 – 1840	478 – 388	552 – 452	3680 – 2920	4240 – 3340
		2930 – 2240	3590 – 2430	974 – 783	1080 – 880	6920 – 5490	7790 – 6070
	5.2	1320 – 1020	1530 – 1150	291 – 242	335 – 281	2230 – 1810	2560 – 2080
		1900 – 1490	2270 – 1610	606 – 497	667 – 562	4350 – 3510	4830 – 3920

momentum cut on the prompt lepton of 10 GeV, all cross sections are reduced to less than 5 pb. The main contribution to large p_T comes from the direct $\gamma\gamma$ process.

VI. CONCLUSIONS

In this paper we have studied the QCD threshold effects on heavy quark production in $\gamma\gamma$ collisions. We have consistently taken into account production by direct and "resolved" photons. We also studied how the cross section depends upon several factors such as quark mass, factorization scale, and choice of the structure functions.

Top quarks are predominantly produced in the direct $\gamma\gamma$ channel. In this case, the $t\bar{t}$ pair is produced through a color singlet channel and the threshold effect results in a substantial enhancement of the total cross section. At $\sqrt{s} = 500$ GeV the enhancement is a factor of 2 for beamstrahlung and more than 1.5 for laser backscattering. For a given collider energy, it will increase with the top mass, while for a given mass it decreases with the collider energy.

For charm and bottom the contributions due to "resolved" photons are dominant, mainly via the once "resolved" $\gamma + \gamma(g)$ process. The effect of the correction is always smaller than the uncertainty due to the choice of the bottom and charm masses.

ACKNOWLEDGMENTS

This work was supported in part by the U.S. Department of Energy under Contract No. DE-AC02-76ER00881, and in part by the University of Wisconsin Research Committee with funds granted by the Wisconsin Alumni Research Foundation. Further support was given by Conselho Nacional de Desenvolvimento Científico e Tecnológico (CNPq) and Fundação de Amparo à Pesquisa do Estado de São Paulo (FAPESP). We would like to thank J. Smith for providing us with the QCD corrections for the charm and bottom production and S. Keller for supplying us with the photon distribution functions. We also thank D. Zeppenfeld for useful discussions. Two of us (O.J.P.E. and S.F.N.) are very grateful to the Institute for Elementary Particle Physics Research, University of Wisconsin – Madison for their kind hospitality during the initial step of this work.

[1] C. Berger *et al.*, Phys. Lett. **86B**, 413 (1979); I. S. Güsken, J. H. Kühn, and P. M. Zerwas, *ibid.* **155B**, 185 (1985); J. Feigenbaum, Phys. Rev. D **43**, 264 (1991); W. Kwong, *ibid.* **43**, 1488 (1991); M. J. Strassler and M. E. Peskin, *ibid.* **43**, 1500 (1991); R. J. Guth and J. H. Kühn, Nucl. Phys. **B368**, 38 (1992).

[2] V. S. Fadin and V. A. Khoze, Pis'ma Zh. Eksp. Teor. Fiz. **46**, 417 (1987) [JETP Lett. **46**, 525 (1987)]; V. S. Fadin

and V. A. Khoze, Yad. Fiz. **48**, 487 (1988) [Sov. J. Nucl. Phys. **48**, 309 (1988)].
[3] V. Fadin, V. A. Khoze, and T. Sjöstrand, Z. Phys. C **48**, 613 (1990).
[4] *Proceedings of the Workshop on Physics and Experiments with Linear Colliders*, Saariselkä, Finland, 1991, edited by R. Orava, P. Eerola, and M. Nordberg (World Scientific, Singapore, in press).
[5] R. J. Noble, Nucl. Instrum. Methods **A256**, 427 (1987).
[6] R. Blankenbecler and S. D. Drell, Phys. Rev. D **36**, 277 (1987); **37**, 3308 (1988); Phys. Rev. Lett. **61**, 2324 (1988); R. Blankenbecler, S. D. Drell, and N. Kroll, Phys. Rev. D **40**, 2462 (1989).
[7] M. Jacob and T. T. Wu, Phys. Lett. B **197**, 253 (1987); Nucl. Phys. **B303**, 373 (1988); **B303**, 389 (1988); **B314**, 334 (1989); **B318**, 53 (1989).
[8] D. V. Schroeder, "Beamstrahlung and QED backgrounds at future linear colliders," Ph.D. thesis, SLAC Report No. 371, 1990.
[9] R. B. Palmer, Annu. Rev. Nucl. Part. Sci. **40**, 529 (1990).
[10] F. R. Arutyunian and V. A. Tumanian, Phys. Lett. **4**, 176 (1963); R. H. Milburn, Phys. Rev. Lett. **10**, 75 (1963).
[11] E. Witten, Nucl. Phys. **B120**, 189 (1977).
[12] M. Drees and R. M. Godbole, Report No. DESY 90-044 (unpublished); Report No. BU 92/1 (unpublished); Phys. Rev. Lett. **67**, 1189 (1991).
[13] F. Halzen, C. S. Kim, and M. L. Stong, Phys. Lett. B **274**, 489 (1992).
[14] V. Barger and R. J. N. Phillips, *Collider Physics* (Addison-Wesley, New York, 1987).
[15] I. F. Ginzburg, G. L. Kotkin, V. G. Serbo, and V. I. Telnov, Nucl. Instrum. Methods **205**, 47 (1983); **219**, 5 (1984); V. I. Telnov, *ibid.* **A294**, 72 (1990).
[16] AMY Collaboration, R. Tanaka *et al.*, Phys. Lett. B **277**, 215 (1992); AMY Collaboration, T. Sazaki *et al.*, *ibid.* **252**, 491 (1990); PLUTO Collaboration, Ch. Berger *et al.*, Z. Phys. C **26**, 353 (1984); Phys. Lett. **142B**, 111 (1984); **149B**, 421 (1984); Nucl. Phys. **B281**, 365 (1987); TASSO Collaboration, H. Althoff *et al.*, Z. Phys. C **31**, 527 (1986); JADE Collaboration, W. Bartel *et al.*, *ibid.* **24**, 231 (1984); CELLO Collaboration, H. J. Behrend *et al.*, in *Proceedings of the XXVth International Conference on High Energy Physics*, Singapore, 1990, edited by K. K. Phua and Y. Yamaguchi (World Scientific, Singapore, 1991); TPC/2γ Collaboration, D. Bintinger *et al.*, Phys. Rev. Lett. **54**, 763 (1985).
[17] H. Abramowicz, K. Charchula, and A. Levy, Phys. Lett. B **269**, 458 (1991).
[18] R. J. DeWitt *et al.*, Phys. Rev. D **19**, 2046 (1979).
[19] M. Drees and K. Grassie, Z. Phys. C **28**, 451 (1985).
[20] D. W. Duke and J. F. Owens, Phys. Rev. D **26**, 1600 (1982).
[21] I. Bigi, Y. Dokshitzer, V. Khoze, J. H. Kühn, and P. M. Zerwas, Phys. Lett. B **181**, 157 (1986).
[22] M. B. Voloshin, Nucl. Phys. **154**, 365 (1979); M. B. Voloshin, Yad. Fiz. **36**, 247 (1982) [Sov. J. Nucl. Phys. **36**, 143 (1982)]; H. Leutwyler, Phys. Lett. **98**, 447 (1981).
[23] K. Fujikawa, Prog. Theor. Phys. **61**, 1186 (1979); I. S. Güsken, J. H. Kühn, and P. M. Zerwas, Nucl. Phys. **B262**, 393 (1985).
[24] A. Sommerfeld, *Atombau und Spektrallinien* (Vieweg, Braunschweig, 1939), Band 2.
[25] A. D. Sakharov, Zh. Eksp. Teor. Fiz. **18**, 631 (1948).
[26] P. Nason, S. Dawson, and R. K. Ellis, Nucl. Phys. **B303**, 607 (1988); P. Nason and R. K. Ellis, *ibid.* **B312**, 551 (1989).
[27] J. Smith and W. L. van Neerven, Nucl. Phys. **B374**, 36 (1992), and references therein.
[28] T. Appelquist and H. D. Politzer, Phys. Rev. D **12**, 1404 (1975).
[29] J. Schwinger, *Particles, Sources and Fields* (Addison-Wesley, New York, 1973), Vol. II.